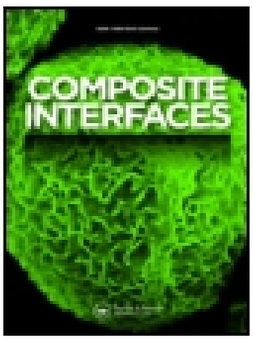

Composite Interfaces

ISSN: 0927-6440 (Print) 1568-5543 (Online) Journal homepage: http://www.tandfonline.com/loi/tcoi20

Magnetic memory effect in magnetite charged polypropylene composite

Ricardo Raúl Mocellini, Osvaldo Agustín Lambri, Damián Gargicevich, Federico Guillermo Bonifacich, Bernd Weidenfeller, Mathias Anhalt & Werner Riehemann

To cite this article: Ricardo Raúl Mocellini, Osvaldo Agustín Lambri, Damián Gargicevich, Federico Guillermo Bonifacich, Bernd Weidenfeller, Mathias Anhalt & Werner Riehemann (2016): Magnetic memory effect in magnetite charged polypropylene composite, Composite Interfaces, DOI: 10.1080/09276440.2017.1250548

To link to this article: http://dx.doi.org/10.1080/09276440.2017.1250548

Published online: 28 Oct 2016.

COMPOSITE INTERFACES, 2016
http://dx.doi.org/10.1080/09276440.2017.1250548

Taylor & Francis
Taylor & Francis Group

Magnetic memory effect in magnetite charged polypropylene composite*

Ricardo Raúl Mocellini[a], Osvaldo Agustín Lambri[a], Damián Gargicevich[a], Federico Guillermo Bonifacich[a], Bernd Weidenfeller[b], Mathias Anhalt[b‡] and Werner Riehemann[c†]

[a]CONICET-UNR, Laboratorio de Materiales, Escuela de Ingeniería Eléctrica, Centro de Tecnología e Investigación Eléctrica, Facultad de Ciencias Exactas, Ingeniería y Agrimensura, Rosario, Argentina; [b]Institute of Particle Technology, Clausthal University of Technology, Clausthal-Zellerfeld, Germany; [c]Institute of Materials Science and Engineering, Clausthal University of Technology, Clausthal-Zellerfeld, Germany

ABSTRACT

The behaviour of damping and dynamic shear modulus in polypropylene charged with either different volume fraction or size of magnetite (Fe_3O_4) particles, as a function of the applied magnetic field at 318, 353 and 403 K; has been studied. An increase of the alternating magnetic field oscillating with 50 Hz, leads to an increase of the damping. In addition, during the subsequently decreasing alternating magnetic field, the damping decreases, but a hysteretic behaviour appeared. The behaviour of the damping and the elastic modulus under the application of an alternating magnetic field was explained by the development of a magnetic fatigue damage occurring around the particle interface due to oscillation of magnetite particles. In contrast, during the increase of a direct magnetic field, the damping decreases and the elastic modulus increases. Measurements performed at 353 and 403 K allowed observing the interaction process among the particles of magnetite in the polymer matrix. After the decrease in the direct magnetic field, from the maximum reached value, damping and modulus remain smaller and higher, respectively; giving rise to a memory effect. In addition, a mesoscopic description of magnetite filled polymer composite materials has been performed in the continuous media by considering the interaction between magnetic and mechanical forces. Theoretical predictions of here developed model were qualitatively applied with good success for explaining the memory effect in magnetite filled polypropylene under the application of a direct magnetic field.

ARTICLE HISTORY
Received 14 July 2016
Accepted 17 October 2016

KEYWORDS
Magnetite-filled polypropylene composite; polymer matrix composite of controllable properties; memory effect; magnetic interaction; mechanical spectroscopy; magnetic field dependence

CONTACT Osvaldo Agustín Lambri olambri@fceia.unr.edu.ar

* We would like to remember our co-author, colleague and friend Werner Riehemann (1952–2016), who died during the preparation of this work after a serious illness in January 2016. Werner was a remarkable researcher of international level. His energy and enthusiasm was a permanent stimulus for our scientific work.

† Passed away.

‡ Present address: FRÖTEK-Kunststofftechnik GmbH, Osterode, Germany.

1. Introduction

Polymer matrix composites (PMC) offer improved physical chemical properties regarding those of the matrix materials, covering a wide range of requirements of stiffness and damping.[1–5] For instance, filler particles like $CaCO_3$ and Fe_3O_4 in polypropylene (PP) matrix composites may improve thermal, mechanical or magnetic properties and influence the activation energies of α', α and β-peaks of the damping spectra.[6–9]

Regarding the magnetic properties of such composites, the isolation of the magnetic particles by the polymer leads to a decrease of power losses in the medium- and high-frequency region compared to classical magnetic materials.[10] Furthermore, a complex shaping of these kind of materials, for example, by injection moulding or other typical plastic processing methods is possible. Thus, magnetic particles embedded in polymeric matrices are used as an electromagnetic interference shield,[11] as power transformers,[12] magnetic cores,[13] stators or other applications,[14] in which alternating magnetic fields are used.

In this work, dynamic mechanical analysis studies conducted under the application of alternating and direct magnetic field have been performed in magnetite charged polypropylene composites. The effects of the alternating and direct magnetic fields on the dynamic response of composite samples were determined. The alternating field leads to a damage of the particle interface, giving rise to a zone of different rheological properties in the PMC around the particles. In contrast, the direct field leads to a movement of the magnetite particle which finally achieves its retention in a metastable state, giving rise to a PMC with modified modulus and damping properties. This effect was here called, the memory effect.

It should be noticed that the magnetite-charged PP composite arise as a damping and stiffness magnetically controllable PMC.

The memory effect involved in this work is different to those in shape memory polymers, where the memory comes from configurational changes at level of the polymer chains.[15]

In order to explain the memory effect in magnetite-charged PP composites, we have developed a model at mesoscopic scale which describes the interaction mechanisms between magnetic particles embedded in polymeric matrix.

2. Experimental

2.1. Materials

As matrix material the polypropylene grade Moplen EP F 31 H (Basell B.V., Klundert, Netherlands) with crystalline melting temperature of TM = 441 K was chosen. The magnetite grade MagniF25 was supplied by Minelco B.V (Rotterdam, Netherlands) with irregular shaped particles with mean diameter of $d = 22$ μm and a wide particle size distribution up to 200 μm.[7,9,16] Polymer and magnetite were mixed in a twin screw extrusion compounder of $D = 25$ mm diameter and a length of $40D$ (ZE25-CL, Berstorff, Germany). Polymer pellets were fed gravimetrically (FlexWall 33, Brabender Technologie, Germany) into the feed throat. At the fifth zone of the extruder, a side feeder was mounted which received the magnetite from another gravimetric dosing system (Soder T20, K-Tron, Germany) and fed it into the molten polymer. The compound left the extruder passing a plate with two holes of 4 mm diameter. The strands were cooled in a water bath and pelletized afterwards. Final samples were prepared using an injection moulding machine (Allrounder 320C 600-250, Arburg, Germany).

The polypropylene samples were charged with 30, 50 and 60 volume percentage of magnetite (Fe_3O_4) particles. Composite samples with 50% vol. magnetite containing particles of mesh 40–63 μm and mesh 63–80 μm were also studied.

2.2. Characterization methods

Dynamic mechanical analysis studies (also called mechanical spectroscopy studies),[17–19] which involve the simultaneous measurement of loss tangent, tan(ϕ) and dynamic shear modulus, G', were performed as a function of the magnetic field strength; in a mechanical spectrometer which was developed and assembled at the laboratory.[20–22] The dynamical response of a linear viscoelastic material is usually described in terms of the complex modulus G^* (or complex compliance J^*) as a function of the circular frequency ω ($\omega = 2\pi f$) and temperature. The complex modulus is generally presented in terms of its real and imaginary parts, that is, $G^* = G' + i\,G''$, where G' is the storage modulus, G'' is the loss modulus and i is the imaginary unit. Consequently, tan(ϕ), also called damping or internal friction, is defined as the quotient between the imaginary and real part of the complex modulus. In addition, a proportionality between G' and the squared natural oscillating frequency can be established. The proportionality constant involves the moment of inertia of the oscillating system and the dimensions of the sample.[23,24]

The spectrometer was operated in torsion, in forced oscillations mode at resonant frequencies of around 10 Hz, under Argon at atmospheric pressure; at three different temperatures: 318, 353 and 403 K (±0.25 K). Damping was determined by measuring the relative half width of the squared resonance peak for a specimen driven into forced vibration using:[17,25,26]

$$\tan(\phi) = \frac{\omega_2 - \omega_1}{\omega_0} \tag{1}$$

where ω_0 is the resonant frequency and ω_1 and ω_2 are the frequencies at which the amplitude of oscillation has fallen to $1/\sqrt{2}$ of the maximum value. Indeed, (1) can be related to the usual expressions for damping, $\tan(\phi) = G''/G' \approx \delta_l/\pi$, where δ_l is the logarithm decrement, by working mathematically the mechanics equations of the movement of the spectrometer and sample.[25,27–29] The use of (1) considering that amplitude of oscillation has fallen to $1/\sqrt{2}$ of the maximum value is particularly important when amplitude dependent damping behaviour appears (doubling the stress does not lead to doubling strain). In fact, the measured value by means of (1) corresponds to the damping value which would be calculated in a specimen when the deformation in space is uniform.[30] So, the contribution to the damping from the spatially inhomogeneous strain distribution in a measured sample at the spectrometer is corrected, i.e., the measured value by (1) corresponds to the intrinsic damping value.[26,30–32] In addition, in mechanical spectrometers working both at resonant frequencies and damping values higher than 10^{-2}, the use of (1) can lead to a increase in the accuracy of the measured value.[26,31,32]

The errors of tan(ϕ) and G', being proportional to the squared oscillating frequency, are less than 2 and 1%, respectively.

The magnetic field was produced by a water-cooled coil device, provided with an electrical heater of compensated windings (Thermocoax, Philips), positioned at the place of the sample. The direction of the applied magnetic field was parallel to the torsion axis.

The maximum amplitude of the used alternating magnetic fields (50 Hz) was H_{AC} = 30 kA/m, while the value of the maximum used direct magnetic field was H_{DC} = 21 kA/m.

Samples were parallelepiped of about 2 mm × 2.2 mm × 30 mm and the maximum oscillating strain on the surface of the sample was 5×10^{-5}.

The measurement of each point of tan(ϕ) as a function of the intensity of the magnetic field involves around 1.5 min, whereupon each value of tan(ϕ) was measured, at least, twice at each field strength. For instance, measuring tan(ϕ) dependent on the magnetic field strength from H_{DC}= 0 kA/m to the maximum field strength of H_{DC} = 21 kA/m needs around half an hour. Decreasing the magnetic field strength is similar time consuming.

3. Theoretical background

3.1. The model

Our here presented model describes the interaction mechanisms between magnetic particles embedded in a polymeric matrix and it uses the following assumptions:

(1) The magnetic particles can be considered as magnetic dipoles. The position of the magnetite particles in the polymeric matrix is fixed and the only freedom of movement is a rotation. In fact, the particles can rotate around their dipole centres (geometric centres) for an alignment in the direction of the applied external magnetic field, Figure 1.

(2) Elastic forces are acting on each dipole caused by elastic properties of the matrix, by magnetic fields of neighbouring magnetic dipoles and by the external magnetic field. Consequently, it is either possible that a dipole returns to the original direction or it remains in a new direction when the external magnetic field is switched off.

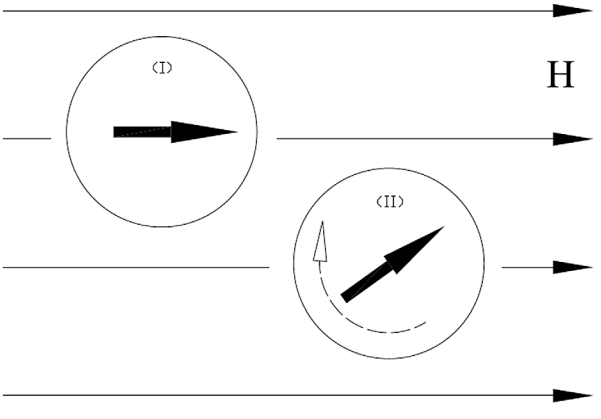

Figure 1. Schematic description of magnetic particles (circles) as magnetic dipoles (arrows) embedded in a material matrix subjected to a magnetic field H. The (I) particle is already aligned in the direction of the external field H. The (II) particle is still rotating around its centre for alignment into the direction of the external magnetic field H. The broken arrow indicates the rotation direction.

3.2. Magneto-mechanical interactions

In this model, we consider three interacting magnetic and mechanical forces whereof two are intrinsic of the material and not dependent on the external magnetic field. The first magneto-mechanical interaction is caused by the magnetic forces between two adjacent particles trying to align them. Secondly, as a consequence of the fixed positions of the centres of the particles, we have to take the deformation of the matrix during the rotation of the dipoles into account. Thus, the second interaction is promoted by an elastic deformation of the matrix. As it can be inferred intuitively, the first and second contributions are counteracting. If the magnetic force tries to rotate a particle into a new position, the force caused by the elastic deformation of the matrix will work against the magnetic force. Finally, the third interaction is caused by the external magnetic field acting on the magnetic particle. The final direction of the particles is reached when all forces are in equilibrium.

3.2.1. Intrinsic moments

3.2.1.1. Magnetic moment contribution. Figure 2 shows a schematic representation of the interaction behaviour of two magnetic particles (I and II) as a function of their geometric arrangement. The particles are lying in two different planes. One particle (I) is assumed to be fixed in a given arbitrary direction and the second one (II) is turning to the same direction due to the magnetic interaction between them. The initial misorientation is θ_0, the distance between the centres of the dipoles is $(2r + d_0)$ and the gap between the dipoles is d_0.

Due to higher attractive than repulsive forces (Figure 2), we will analyse the attractive case between the dipoles. This consideration is valid for a mean field approximation describing the interaction process in a continuous medium.

The magnetostatic force F_m gives rise to a torsional moment M_m which promotes the alignment of two magnetic particles [33]

$$M_m = F_m \cdot \cos(\xi) \cdot 2r \tag{2}$$

where $F_m = R_1/d_1^2$, $R_1 = p_1 \cdot p_2/4\pi\mu_0$, $p_1 = p_2 = p$ are the poles strength, μ_0 is the permeability of vacuum and d_1 is the separation between the poles of different charge.

By working with the sine theorem, we can write the cos(ξ) in (2), corresponding to Figure 2, as a function of angles θ, θ_0, θ_a; in the form

$$\cos(\xi) = \frac{a}{d_1} \sin\left(\theta_a + \theta_0 - \theta\right) \tag{3}$$

Consequently, the torsional moment in (2) can be written as follows:

$$M_m = R_1 \frac{2ra}{d_1^3} \sin\left(\theta_a + \theta_0 - \theta\right) \tag{4}$$

In the following paragraphs we describe all angles and distances given in Figure 2 as functions of the angles θ, θ_0, θ_c. The distance d_1 can be obtained using the cosine theorem.

$$d_1^2 = a^2 + r^2 - 2ar\cos\left(\theta_a + \theta_0 - \theta\right) \tag{5}$$

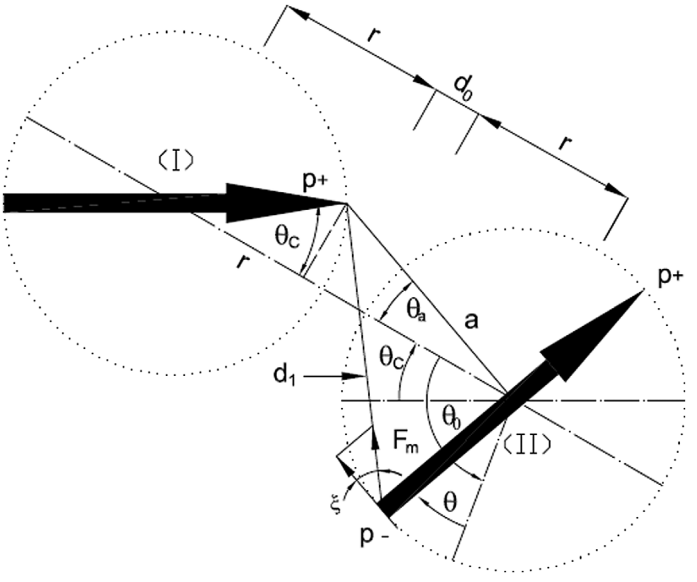

Figure 2. Geometric representation of the magnetic moments for the basic unit in the mean field approximation used in the present work.

Likewise, the distance a can be described using the triangles described by a, r and $(2r + d_0)$ as a function of the θ_a, as follows:

$$a^2 = r^2 - \left(2r + d_0\right)^2 + 2a\left(2r + d_0\right)\cos\left(\theta_a\right) \tag{6}$$

or using the same triangle but now considering a and θ_c, we can write

$$a^2 = r^2 + \left(2r + d_0\right)^2 - 2r\left(2r + d_0\right)\cos\left(\theta_c\right) \tag{7}$$

By rearranging, we obtain

$$a^2 = 4r^2\left[\frac{5}{4} + \frac{1}{4}\left(\frac{d_0}{r}\right)^2 + \frac{d_0}{r} - \left(1 + \frac{1}{2}\frac{d_0}{r}\right)\cos\left(\theta_c\right)\right] \tag{8}$$

and by defining $\rho = \left(\frac{d_0}{r}\right)$, we can write

$$a = 2r\left[\frac{1}{4}\rho^2 + \rho + \frac{5}{4} - \left(1 + \frac{1}{2}\rho\right)\cos\left(\theta_c\right)\right]^{\frac{1}{2}} \tag{9}$$

Then, we can obtain θ_a as a function of θ_c by relating (6) and (7):

$$\theta_a = \cos^{-1}\left\{\frac{\left[\left(1 + \frac{1}{2}\rho\right) - \frac{1}{2}\cos\left(\theta_c\right)\right]}{\sqrt{\frac{1}{4}\rho^2 + \rho + \frac{5}{4} - \left(1 + \frac{1}{2}\rho\right)\cos\left(\theta_c\right)}}\right\} \tag{10}$$

Inserting (8) and (10) into (5) the distance d_1 as a function of the angular variables equals.

$$d_1 = \left\{ \begin{array}{l} 4r^2\left[\frac{1}{4}\rho^2 + \rho + \frac{5}{4} - \left(1+\frac{1}{2}\rho\right)\cos\left(\theta_c\right)\right] + r^2 - \\ 4r^2\left[\frac{1}{4}\rho^2 + \rho + \frac{5}{4} - \left(1+\frac{1}{2}\rho\right)\cos\left(\theta_c\right)\right]^{\frac{1}{2}} \cos\left(\theta_a + \theta_0 - \theta\right) \end{array} \right\}^{\frac{1}{2}} \tag{11}$$

Finally, as θ_a is a function of θ_c, we can obtain a general expression for the torsional moment (4) as a function of θ_0, θ_c and θ, in the form

$$M_m = R_1 \frac{4r^2\sqrt{\frac{1}{4}\rho^2 + \rho + \frac{5}{4} - \left(1+\frac{1}{2}\rho\right)\cos\left(\theta_c\right)}\sin\left(\theta_a + \theta_0 - \theta\right)}{\left\{4r^2\left[\frac{1}{4}\rho^2 + \rho + \frac{5}{4} - \left(1+\frac{1}{2}\rho\right)\cos\left(\theta_c\right)\right] + r^2 - 4r^2\left[\frac{1}{4}\rho^2 + \rho + \frac{5}{4} - \left(1+\frac{1}{2}\rho\right)\cos\left(\theta_c\right)\right]^{\frac{1}{2}}\cos\left(\theta_a + \theta_0 - \theta\right)\right\}^{\frac{3}{2}}} \tag{12}$$

In the following paragraphs, (12) is evaluated for different values of θ_c and it will be shown that M_m does not significantly change. Indeed, the curve shapes of plots M_m against θ are not identical for different values of θ_c, but the characteristics of the plot is similar shaped, as it can be seen in Figure 3. Thus, and additionally for the reasons of a more simple mathematical treatment, we will concentrate on particles which are lying in the same plane ($\theta_c = 0$). This simplification does not diminish the applicability of the model, since in the real matrix the particles are randomly spread having different dependences of M_m versus θ but all of them with similar characteristics as it is shown in Figure 3. In a continuous media containing randomly spread magnetic particles, interaction processes occur at different values of θ_c. Consequently, considering a mean field approximation the assumption of $\theta_c = 0$ can be reasonable.

Therefore, we introduce here the so-called equivalent dipole, which is composed of two particles having their centres on the same plane ($\theta_c = 0$, Figure 4). One of them is fixed in a given direction, and the other one is free to rotate for aligning. Considering $\theta_c = 0$ and $R_2 = R_1/(2r)^{1/2}$, (12) can be rearranged to

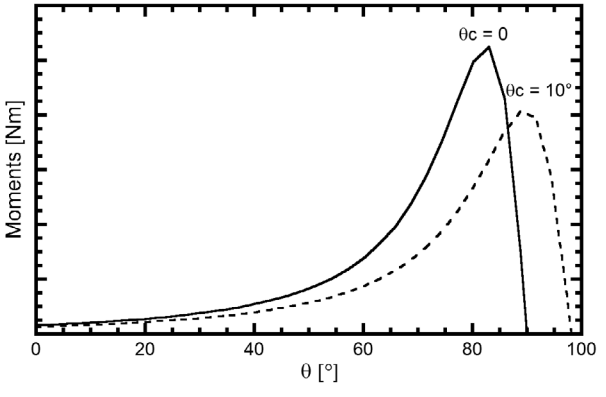

Figure 3. Response of (12), assuming arbitrary values such that: $\rho = 0.2$, $r = 1$, $\theta_0 = 90°$ and $R_1 = 1$.

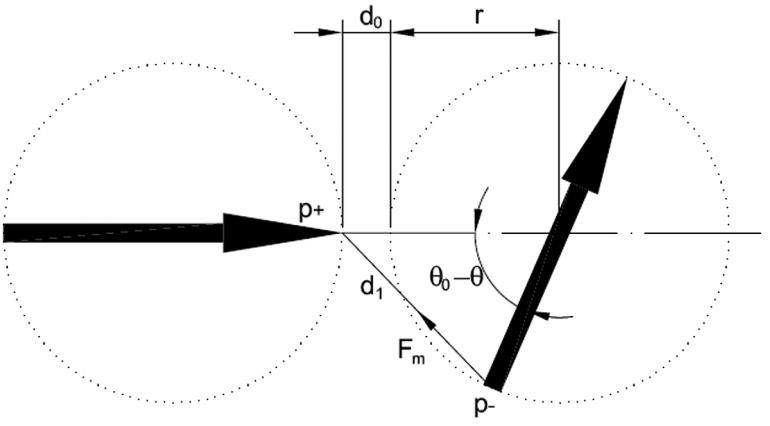

Figure 4. Equivalent dipole arrangement, aligned between them ($\theta_c = 0$).

$$M_m = \frac{R_2}{\sqrt{\rho+1}} \frac{\sin\left(\theta_0 - \theta\right)}{\left[\frac{\frac{\rho^2}{2}+\rho+1}{\rho+1} - \cos\left(\theta_0 - \theta\right)\right]^{\frac{3}{2}}} \tag{13}$$

The behaviour of M_m, (13), as a function of θ for different values of $\rho = \left(d_0/r\right)$ and for $\theta_0 = 90°$ is shown in Figure 5. In addition, the behaviour of M_m as a function of θ for different values of θ_0 (30°, 60° and 90°) and for an arbitrary constant value of ρ is plotted in Figure 6.

In summary, with (13) we have obtained a mathematical expression describing the magnetic interaction between two neighbouring particles embedded in an ideal elastic medium without elastic constants. In fact, as it can be seen from Figures 5 and 6, the torsional moment increases nearly until the alignment is reached, both for different θ_0 and ρ.

3.2.1.2. Elastic moment contribution. If the matrix in which the particles are embedded has given elastic moduli an interaction counteracting the particle alignment will arise which tries to turn back the particles into the original position.

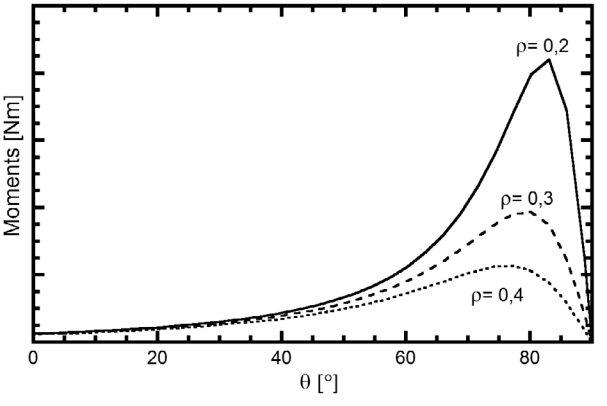

Figure 5. Behaviour of M_m, (13) as a function of θ for different values of $\rho = d_0/r$ and for $\theta_0 = 90°$.

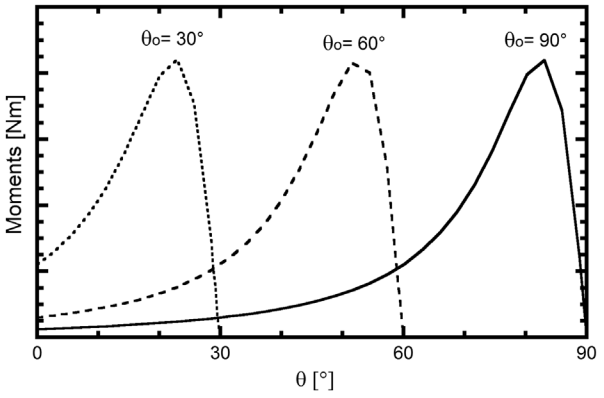

Figure 6. Behaviour of M_m, (13) as a function of θ for θ_0: 30°, 60° and 90°. $\rho = d_0/r = 0.2$.

In order to analyse the deformation of the elastic matrix promoted by the rotation of the particle, the following assumptions are made:

(1) The magnetic particle is assumed to be a sphere.
(2) The thickness of the elastically deformed zone of the matrix (interphase) around the dipole equals the mean distance between two neighbouring particles (d_0). This is schematically shown in Figure 7(a) and (c).

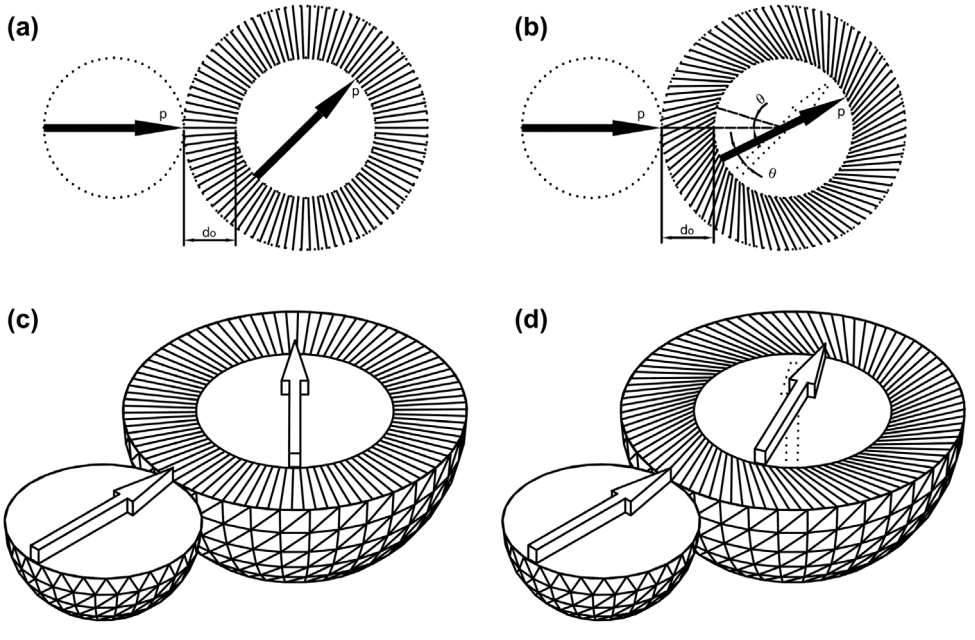

Figure 7. Schematic illustration of an interface (dashed zone) between two spherical dipoles, which is elastically deformed by the rotation of the dipole.

(3) The outer layer of the interphase shown in Figure 7(a) is considered to be fixed to the matrix and not deformed.
(4) The surface of the magnetic particle and the surrounding matrix are firmly linked together in such a way, that a rotation of the particle leads to a deformation of the matrix which is schematically shown by the interphase (dashed zone) in Figure 7(b) and (d).

A complex deformation mode can be separated into two single deformation modes, such as tensile and shear deformations.[34] Thus, these both deformation modes will be considered in the following paragraphs to describe the deformation process of the interface, which is an approximated solution to the real deformation state shown in Figure 7.

For analysing the tensile deformation mode, we consider a distance of initial length d_0 in the interphase, which is stretched up to d_2 as a consequence of the rotation of the particle by an angle θ (Figure 8).

From geometric and angular relationships

$$d_2^2 = \left(d_0 + r\right)^2 + r^2 - 2\left(d_0 + r\right) r\cos\left(\theta\right) \text{ and } d_2^2 = r^2(\rho+1)\left[\frac{\rho^2 + 2\rho + 2}{(\rho+1)} - 2\cos\left(\theta\right)\right] \tag{14}$$

can be deduced and d_2 equals

$$d_2 = r\sqrt{\rho^2 + (2\rho+2)(1-\cos\left(\theta\right))} \tag{15}$$

With the usual definition of strain $\varepsilon = \Delta d/d_0 = d_2/d_0 - 1$ and by replacing of d_2/d_0 by the expression for d_2 given by (15), we have

$$\varepsilon = \sqrt{1 + \left(\frac{2}{\rho^2} + \frac{2}{\rho}\right)(1-\cos\left(\theta\right))} - 1 \tag{16}$$

Using the elastic moment generated by the tensile strain on the elastic matrix, $M = 2rF$, and Hooke's law, we obtain

$$M = 2rAE\varepsilon \tag{17}$$

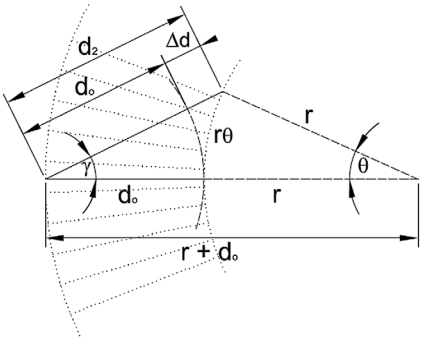

Figure 8. Representation of geometric data by an elastic tensile deformation of the interface.

wherein A is the area of a half sphere, E is the Young's modulus, r is the average radius of particles and ε is the tensile strain.

By replacing the value of ε given by (16) in (17), we can obtain the elastic moment promoted by a tensile state as a function of the torsion angle θ to be

$$M_{kE} = 4\pi r^3 E\left(\sqrt{1+\left(\frac{2}{\rho^2}+\frac{2}{\rho}\right)(1-\cos(\theta))}-1\right) \tag{18}$$

After analysing the tensile deformation mode with (18), we will now examine the shear deformation mode. The deformation of interphase (Figure 7) is caused by a pure shear strain (Figure 9).

Using Hooke's equation for the case of shear deformation and considering a half sphere with area $2\pi r^2$ just as in the case of tensile deformation (Figure 9), the elastic moment is

$$M_{kG} = G\frac{4\pi r^3}{\rho}\theta \tag{19}$$

Finally, by adding the contributions of tensile and shear deformation, we obtain the whole elastic moment related to the deformation of the interface promoted by the rotation of the dipole:

$$M_{G'} = M_{kE} + M_{kG} = 4\pi r^3 E\left(\sqrt{1+\left(\frac{2}{\rho^2}+\frac{2}{\rho}\right)(1-\cos(\theta))}-1\right) + G\frac{4\pi r^3}{\rho}\theta \tag{20}$$

3.2.1.3. Whole intrinsic contribution. The total intrinsic interaction is the sum of the magnetic interaction and the elastic contribution, i.e., the algebraic sum of (13) plus (20). We are speaking of algebraic sum because the counteracting forces lead to opposite signs of magnetic and elastic interaction. We use the positive sign for the magnetic moment when the rotation is clockwise. The whole intrinsic magnetomechanical moment has the form

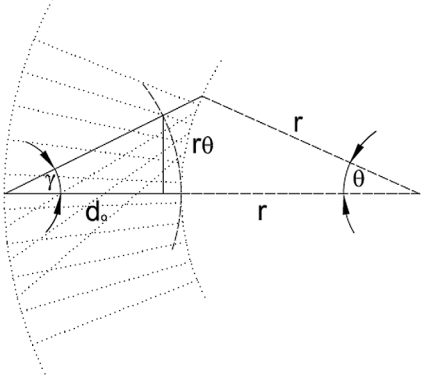

Figure 9. Representation of geometric data by an elastic shear deformation of the interface.

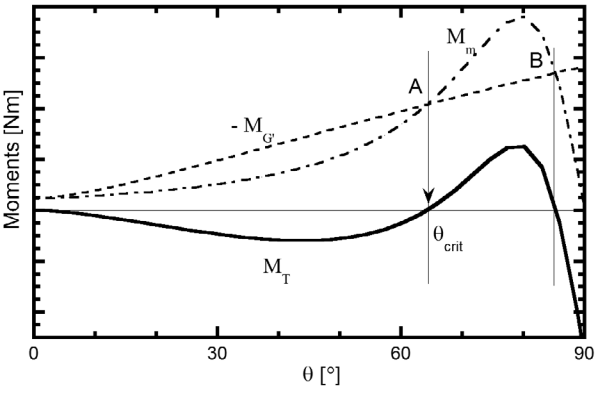

Figure 10. Plot of elastic $M_{G'}$, magnetic M_m and total moments ($M_T = M_m - M_{G'}$) as a function of the orientation angle θ. The curve of elastic moment $M_{G'}$ has been plotted multiplied by (−1) in order to show clearer the angle (θ_{crit}) where the total moment equals zero or where in our plot the intersection (labelled with A) between the magnetic and elastic moment occurs.

$$M_T = -4\pi r^3 E\left(\sqrt{1+\left(\frac{2}{\rho^2}+\frac{2}{\rho}\right)(1-\cos(\theta))}-1\right) - G\frac{4\pi r^3}{\rho}\theta + \frac{R_2}{\sqrt{\rho+1}}\frac{\sin\left(\theta_0-\theta\right)}{\left[\frac{\frac{\rho^2}{2}+\rho+1}{\rho+1}-\cos\left(\theta_0-\theta\right)\right]^{\frac{3}{2}}} \tag{21}$$

The elastic, magnetic and total moments as a function of the orientation angle θ are plotted in Figure 10. It can be seen that the total moment equals zero at a critical angle θ_{crit} (labelled with *A* in Figure 10). For rotation angles higher than θ_{crit}, the system is unstable, and the particle rotates until the angle of the stable position (labelled with B in Figure 10) is reached.

3.2.1.4. Energy study. To simplify the analytical integration of expression (21), the elastic term which is related to the Young modulus has been re-written (approach to the first term as it is shown in the Appendix 1), that is

$$M_T = -11.6\pi r^3 E\theta - G\frac{4\pi r^3}{\rho}\theta + \frac{R_2}{\sqrt{\rho+1}}\frac{\sin\left(\theta_0-\theta\right)}{\left[\frac{\frac{\rho^2}{2}+\rho+1}{\rho+1}-\cos\left(\theta_0-\theta\right)\right]^{\frac{3}{2}}} \tag{22}$$

Using the general equation ($E = \int M d\theta$) for the relation between energy and the magnetic moment with respect to the rotation angle θ, the energy takes the form.[35]

$$E_T = \frac{1}{2}\left(11.6\pi r^3 E + G\frac{4\pi r^3}{\rho}\right)\theta^2 - \frac{R_2}{\sqrt{\rho+1}}\frac{2}{\left[\frac{\frac{\rho^2}{2}+\rho+1}{\rho+1}-\cos\left(\theta_0-\theta\right)\right]^{\frac{1}{2}}} \tag{23}$$

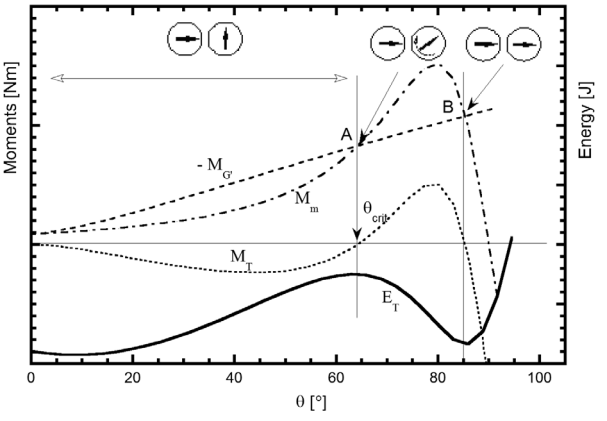

Figure 11. Dependence of the magnetic and mechanical moments ($M_{G'}$, M_m, $M_T = M_m - M_{G'}$) and the energy (E_T) on the rotation angle θ. Again the curve of elastic moment $M_{G'}$ has been plotted multiplied by (−1; Figure 10). In the top of the Figure 11 dipole orientations at various angles θ are schematically shown.

Figure 11 shows the energy E_T as a function of the angle θ. At the critical angle θ_{crit}, an unstable state of energy occurs, as it could be expected. In the top of Figure 11 particle orientations are schematically shown. At torsion angles higher than θ_{crit}, the particles rotate as a consequence of the magnetic interaction into a parallel state (indicated by point B in figure). This stage is represented by an energy minimum at which the particles have reached a new equilibrium position.

3.2.2. External field

The third interaction process is related to the interaction between the particles and an external magnetic field. We consider two particles embedded in a non-magnetic matrix as it is shown in Figure 12. The magnetic force is defined in the usual form, $F_H = pH$, where

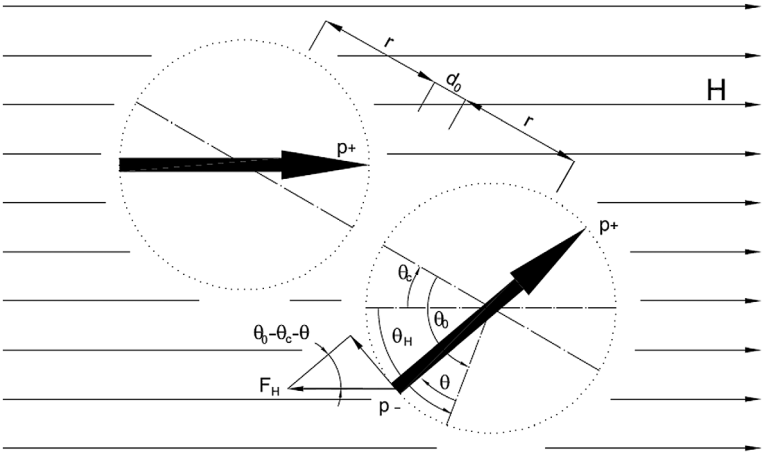

Figure 12. Schematic behaviour of two magnetic dipoles embedded a non-magnetic matrix in an external magnetic field H.

p is the magnetic mass (magnetic strength) of the dipolar moment of the particle and H is the external magnetic field.[33] As it can be shown, the magnetic moment promoted by the external field is given by

$$M_H = 2rpH \sin\left(\theta_H - \theta\right) \tag{24}$$

wherein the angle θ_H is the difference between the angular position θ_0 at the original state and the angular position θ_c which is reached after the alignment of the particles. Then, the total magnetomechanical moment in an external magnetic field and with consideration of the intrinsic moments takes the form

$$\begin{aligned} M_{Tot} = & -4\pi r^3 E\left(\sqrt{1+\left(\frac{2}{\rho^2}+\frac{2}{\rho}\right)(1-\cos(\theta))}-1\right) \\ & - G\frac{4\pi r^3}{\rho}\theta + \frac{R_2}{\sqrt{\rho+1}}\frac{\sin\left(\theta_0-\theta\right)}{\left[\frac{\frac{\rho^2}{2}+\rho+1}{\rho+1}-\cos\left(\theta_0-\theta\right)\right]^{\frac{3}{2}}} \\ & + 2rpH\sin\left(\theta_H-\theta\right) \end{aligned} \tag{25}$$

Using the linear approximation from Appendix for the elastic contribution, a more friendly equation for mathematical calculations can be obtained, that is:

$$M_{Tot} = -11.6\pi r^3 E\theta - G\frac{4\pi r^3}{\rho}\theta + \frac{R_2}{\sqrt{\rho+1}}\frac{\sin\left(\theta_0-\theta\right)}{\left[\frac{\frac{\rho^2}{2}+\rho+1}{\rho+1}-\cos\left(\theta_0-\theta\right)\right]^{\frac{3}{2}}} + 2rpH\sin\left(\theta_H-\theta\right) \tag{26}$$

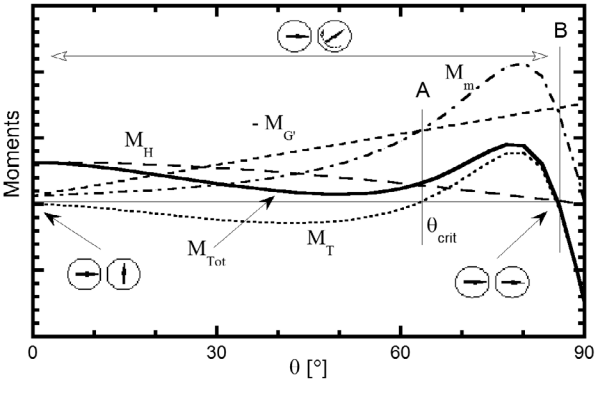

Figure 13. The elastic moment $M_{G'}$ (dashed line), the magnetic moment M_m (dash-dot line), the total intrinsic magnetomechanical moment $M_T = M_m - M_{G'}$ (dotted line), the magnetic moment M_H promoted by the external field (long dashed line) and the total magnetomechanical moment M_{Tot}, (full line), as a function of the rotation angle θ; are shown. Again the curve of elastic moment $M_{G'}$ has been plotted multiplied by (−1) (Figure 10).

The behaviour of M_{Tot} as a function of the rotation angle θ is shown in Figure 13. The external magnetic moment is the driving force which moves the particles from the original position towards the aligned position reached at position B. Indeed, the moment is now positive over the θ angles up to the B value, where the M_{Tot} changes its sign. Therefore, the mobile particle will be in an unstable position until the θ value corresponding to position B is reached, see particles and double headed arrow on top of the Figure 13.

4. Results and discussion

Some of the results reported for magnetite-charged PP under alternating magnetic field were already reported in Ref. [8], but they are included here in order to improve the discussion and understanding of the present work. In fact, in the present work these already reported results are shown together with new ones, completing the experimental study; mainly regarding the experiments under alternating field at higher temperatures.

Figure 14 shows the tan(ϕ) behaviour as a function of the H_{AC} amplitude during the first magnetic cycle for samples with different volume fractions of magnetite. A magnetic cycle involves the increase of H_{AC} from zero to a maximum value and the subsequent decrease to zero. As it can be seen from the figure, during the first increase of alternating magnetic field H_{AC}, tan(ϕ) increases for all samples (full symbols). During the subsequent decreasing of the magnetic field H_{AC}, tan(ϕ) decreases, too (empty symbols). For all magnetic fields H_{AC}, the tan(ϕ) values during the decreasing part of the magnetic cycle are smaller than for the previously increasing part, i.e., a hysteresis in the damping response has appeared.

In the other hand, during the first increase of the magnetic field amplitudes H_{AC}, the elastic shear modulus, G', decreases for all tested samples. In addition, during the subsequent

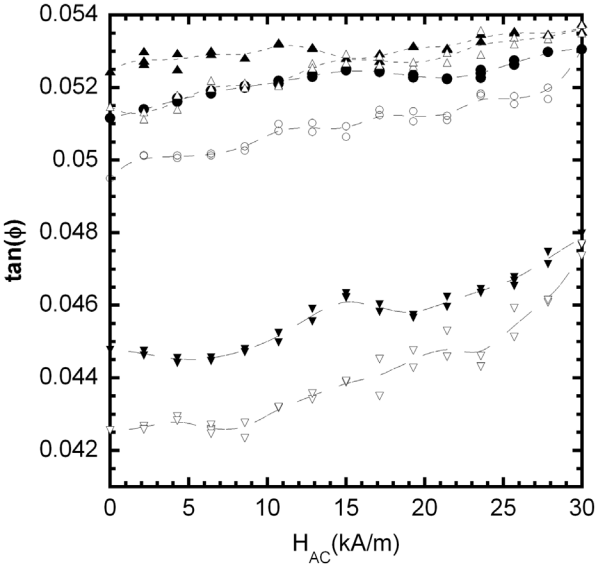

Figure 14. Damping as a function of magnetic field amplitude, alternating with 50 Hz during the first magnetic cycle, measured at 318 K, for polypropylenes with different volume fractions of magnetite. Full symbols increasing part of magnetic cycle. Empty symbols decreasing part of magnetic cycle. Triangles: 30%, circles: 50%, inverted triangles: 60%. Lines on the curves represent an average behaviour.

Table 1. Changes in $\Delta G'$ and $\Delta\tan(\phi)$ during the magnetic cycles at 318 K.

Sample PP + *X*% vol. Fe_3O_4/unsieved	Alternate H, H_{AC}		$\Delta\tan(\phi)$ (%) at $H_{AC}=0$ after the first magnetic cycle	Direct H, H_{DC}	
	Values between zero and the maximum magnetic field in the first increasing run of the magnetic field			Values between zero and the maximum magnetic field in the first increasing run of the magnetic field	
	$\Delta G'$ (%)	$\Delta\tan(\phi)$ (%)		$\Delta G'$ (%)	$\Delta\tan(\phi)$ (%)
30	−7.1	2	−1	~0.1 (*)	−1
50	−7.5	3	−3	~0.1 (*)	−2
60	−10	8	−5	0.3	−3
Sample PP + 50% vol. Fe_3O_4/Mesh					
40–63	−7.4/−7.5	3	−3	~0.1 (*)	−2
63–80	−7.5	3	−3	~0.2 (*)	−2

Notes: Changes in the dynamic elastic shear modulus $\Delta G'$, and in the damping, $\Delta\tan(\phi)$, during part of the magnetic cycles, at 318 K. (*) this variation cannot be assured completely and it must be considered with care.

decrease in the magnetic field, G' increases again and a hysteresis behaviour could not be observed for all the checked samples.

Table 1 summarizes the percentage changes of damping and modulus corresponding to the whole variation in H_{AC}.

The physical mechanism controlling the behaviour of damping and modulus as a function of the H_{AC} strength during the magnetic cycles, was reported in a previous work.[8] Indeed, the behaviour of damping as a function of the magnetic field during the magnetic cycles was explained considering both an effect of modification of the mechanical properties and local damage of the polymer matrix around the particles of magnetite. Indeed, a small rotation of the magnetite particles relative to the matrix polymer promoted by the oscillating magnetic field causes an additional frictional contribution to the mechanical damping of the whole PP matrix, leading to the increase in the $\tan(\phi)$ values, as the intensity of the alternating magnetic field increases. This can be related to the modification of the surrounding matrix part of the oscillating particles due to the magnetic force, giving rise to a more viscous zone around the inclusions. In addition, the heating of the particles due to the alternating magnetic field can contribute to the mechanism above-mentioned.[8] Besides, the modulus does not exhibit a hysteretic behaviour due to the degree of damage of the inclusion's surrounding matrix does not affect irreversibly and substantially the measured elastic modulus, since the particles are still bonded to the polymer matrix.[8]

It can be also seen from Figure 14 that both the damping curves decrease as the volume fraction of magnetite increases and the increase of the damping with rising magnetic field is smaller as the volume fraction is smaller. In addition, the area involved in the cycles decreases as the volume fraction of inclusions decreases.

The behaviour exhibited by the $\tan(\phi)$ in Figure 14 is in agreement with the above assumption about a magnetically controlled local modification of the rheological state of the polymer matrix in the surrounding zone around the magnetite inclusions. In fact, a larger concentration of magnetite gives rise to a larger quantity of more viscous modified zones which increase the damping as the alternating magnetic field is increased.[8] It leads to an increase in the mean slope $\Delta\tan(\phi)/\Delta H$ of damping curve as a function of the alternating magnetic field. The mean slope values of the damping curves are also listed in Table 1.

The decreasing tan(ϕ) with increasing magnetite volume fraction can be explained easily from the point of view of a composite material. In fact, as the volume fraction of magnetite, which has higher modulus and smaller damping capacity, increases; the damping of composite material will decrease.

The larger areas in the hysteretic curves of tan(ϕ) for larger volume fraction of magnetite is also in agreement with the mechanism above-proposed. Indeed, the larger concentration of magnetite leads to a larger amount of surrounding zones around the magnetite particles suffering a local modification of their rheological state.

tan(ϕ) and G' measurements performed on samples with 50% vol. of magnetite but with different particles sizes, mesh 40–63 μm and mesh 63–80 μm, did not show clear differences in comparison to the polypropylene samples filled with unsieved magnetite particles, see Table 1.

It should be highlighted that, an increase in temperature for measuring the magnetic cycles (H_{AC}) leads to a decrease in the area of the hysteresis in tan(ϕ) for all the studied samples. For each kind of sample the decrease in its hysteresis area is around 0.8, and 0.3% at 353 and 403 K, respectively. The decrease in the area of hysteresis in tan(ϕ) as the temperature increases can be explained considering that an increase in temperature leads to an increase in the chain polymer mobility (decrease in the elastic modulus). Then, the matrix can room easier the stresses promoted by the rotation of the magnetite particles under the H_{AC} solicitation giving rise to a less modified interface between the polymer and the particle, involving also less amount of debonding at the interface.

On the other hand, the response of the studied samples to the application of a directional magnetic field was completely different to the previous showed case, concerning to the alternating magnetic field. In fact, the response can be explained qualitatively on the basis of the theoretical work developed in Section 'Theoretical Background'.

Measurements performed at 317 K, leads to the damping decreases and the modulus increases, as the applied H_{DC} field increases, for all the studied samples. In Table 1, the changes of damping and modulus for this case, are also shown. A hysteretic behaviour of tan(ϕ) and shear modulus G' could not be detected. Therefore, we can propose that a modification of the rheological state of the polymer matrix or a damage, in the surrounding of the magnetite inclusions do not appear when the sample is subjected to a directional (DC) magnetic field, within the studied range of intensity, at 317 K. Nevertheless, the behaviour of both damping and modulus during the magnetic cycle, under H_{DC}, change markedly with a temperature increase.

Figures 15 and 16 show the damping and the elastic modulus measured at 353 and 403 K, for a sample with 50% vol. magnetite, unsieved, respectively. Full and empty symbols show the values measured during the increase in H_{DC} and its subsequent decrease, respectively. As it can be seen from the figures, the modulus increases, while, the damping decreases; as H_{DC} increases. Plotted values in Figures 15 and 16 are the average of two measured points at each field strength.

The exhibited behaviour of damping and modulus during the increasing of the H_{DC} external magnetic field can be easily explained, considering that the field induces stresses on the magnetite particles embedded into the matrix reducing the mobility of the polymer chains. In fact, the applied H_{DC} field attempts to rotate the particles leading to an increase in the internal stresses into the polymer matrix which decreases the mobility of polymer chains; giving rise to both the increase in modulus and the decrease in damping.

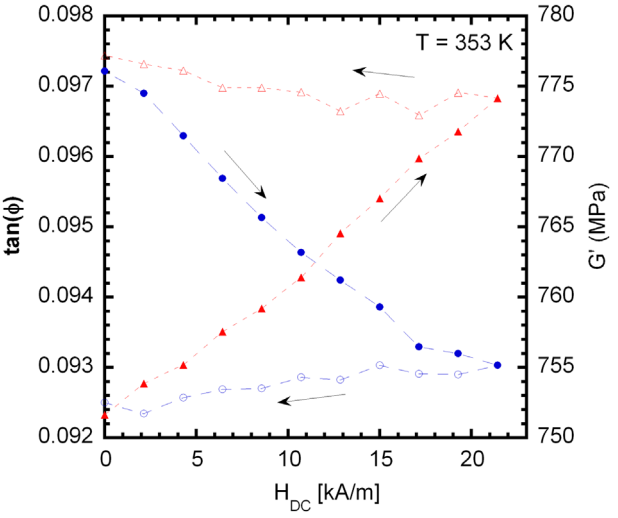

Figure 15. Damping and dynamic shear modulus measured at 353 K for a magnetite (50% vol.) filled PP sample. tan(ϕ): Circles and G': Triangles. Full symbols: Values measured during increasing H_{DC}. Empty symbols: Values measured during decreasing H_{DC}. Arrows indicate the increase and decrease runs in H_{DC}. Lines represent a guide for the eyes.

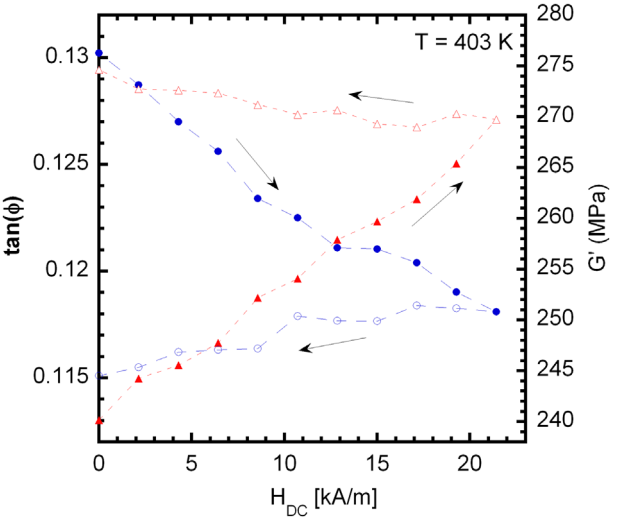

Figure 16. Damping and dynamic shear modulus measured at 403 K for a magnetite (50% vol.) filled PP sample. tan(ϕ): Circles and G': Triangles. Full symbols: Values measured during increasing H_{DC}. Empty symbols: Values measured during decreasing H_{DC}. Arrows indicate the increase and decrease runs in H_{DC}. Lines represent a guide for the eyes.

This situation can be easily understood on the basis of dislocations theory. Indeed, when internal stresses increase the energy valley to overcome by the dislocation line is higher and then the dislocation mobility is decreased.[36] In addition, the relation of the polymer chains to dislocation lines arises after the study of the viscoelastic behaviour of polymers in earlier times.[37,38]

Nevertheless, during the decrease in H_{DC} both modulus and damping remain exhibiting the last value reached at the highest field strength, the so-called memory effect (see Figures 15 and 16). In fact, the higher values of modulus and the smaller values of damping remained during the decrease in the field strength are indicating that the sample is thermodynamically in an energy valley which is higher than the corresponding to the initial zero strength field. So, the polymer chains are stressed, leading to a decrease in their mobility, giving rise to both smaller and higher values of damping and elastic modulus, respectively. It should be stressed that, these results are in qualitative agreement with the theoretical prediction of our model regarding the appearance of another possible energy valley with higher energy, see Figures 11 and 12. In fact, as it was shown in Figure 11, when the particle rotates up to θ_{crit}, it gives rise to nil moment M_T (see A point in the figure) and then it leads to a saddle point in the energy behaviour. Consequently, the particles in such position are able to move involving rotation until that a new equilibrium position is achieved (see B point in the figure). Therefore, B position is another (meta)-stable place with higher energy than the original state, and then particles are now retained in this new position.

It is convenient to be mentioned here, that the real rotation angle involved in the magnetite particles embedded in the polypropylene matrix is much smaller than the cases shown in Section 'Theoretical Background'. Indeed, we are referring to rotation angles which come from small misorientations regarding the direction of the direct field. In fact, the experiments conducted under alternating magnetic field confirm a rotation of the particles with an enough angle to damage the neighbourhood zone of the particles.

The difference of the behaviour between measurements under H_{DC} at room temperatures and at higher temperatures is controlled by the decrease of elastic modulus as the temperature increases. The elastic modulus decrease as the temperature increases, enhancing the capability of particle rotation due to a smaller restoration capability of the matrix. In fact, at around 270 K a marked decrease in the modulus starts in magnetite charged polypropylene due to the development of the α and α' relaxations.[3,5]

Moreover, when a direct magnetic field is applied (see Figure 13) the magnetic field enhances the rotation of particles up to the B point; due to the M_T curve is shifted upwards. Consequently, it leads to the sample to a higher energy state, even after the decrease of H_{DC}. The polymer chains are retained with a less mobility arrangement, giving rise to the memory effect of damping and modulus as the H_{DC} field decreases, see Figures 15 and 16.

5. Conclusions

The behaviour of the damping and the dynamic shear modulus in polypropylene–magnetite composites filled with different volume fractions of magnetite particles, at 318, 353 and 403 K, was studied as a function of the applied magnetic field.

An increase and subsequent decrease of the alternating magnetic field leads to hysteretic behaviour of the damping promoted by fatigue damage around the particle interface due to oscillation of magnetite particles.

In contrast, the application of a direct magnetic field, at 318 K, increases the shear modulus, while the damping is reduced, which is the result of stresses generated by magnetite particles reducing the mobility of polymer chains. Moreover, a decrease in the elastic modulus, due to an increase in temperature, allowed observing the interaction process between the particles of magnetite in the polymer matrix, giving rise to the so-called memory effect.

Indeed, after the decrease in the direct magnetic field, from the maximum reached value, for magnetic cycles performed at temperature of 353 and 403 K, damping and modulus remain smaller and higher, respectively. Therefore, the magnetite-charged polypropylene can be considered as a polymer matrix composite exhibiting controllable both damping and stiffness by the applied direct magnetic field.

A mesoscopic description of magnetite filled polymer composite materials has been performed in the continuous media by considering the interaction between magnetic and mechanical forces. Magneto-mechanical interaction is caused by both the magnetic forces between two adjacent particles trying to align them and an elastic deformation of the matrix which is counteracting. Theoretical predictions successfully explain in a qualitative mode the memory effect in magnetite-filled polypropylene composite under the application of a direct magnetic field.

Disclosure statement

No potential conflict of interest was reported by the authors.

Funding

This work was supported by the CONICET-PIP [grant number 179CO], [grant number 2098]; PID-UNR [grant number ING 450], [grant number ING 453], 2014–2017; Collaboration Agreement between the Clausthal University of Technology and the Universidad Nacional de Rosario [grant number 2292/2015], 2013 and 2015.

References

[1] MIL-DBK-17-3F. Composite materials handbook volume 3. Polymer matrix composites materials usage, design, and analysis. Department of defense handbook. Department of Defense. Washington (DC); 2002.
[2] Mark JE, editor. Polymer data handbook. New York (NY): Oxford University Press; 1999.
[3] Gauthier MM, editor. Engineered materials handbook desk edition. Materials Park: ASM International; 1995.
[4] Harris CM, Crede CE, editors. Shock and vibration handbook. New York (NY): McGraw Hill; 1961.
[5] Lahelin M, Aaltio I, Heczko O, et al. DMA testing of Ni–Mn–Ga/polymer composites. Comp Part A. 2009;40:125–129.
[6] Li Y, Fang QF, Yi ZG, et al. A study of internal friction in polypropylene (PP) filled with nanometer-scale $CaCO_3$ particles. Mater Sci Eng A. 2004;370:268–272.
[7] Weidenfeller B, Riehemann W, Lei Q. Mechanical spectroscopy of polymer magnetite composites. Mater Sci Eng A. 2004;370:278–283.
[8] Lambri OA, Gargicevich D, Tarditti F, et al. Magnetic field dependent damping of magnetic particle filled polypropylene. Solid State Phenom. 2012;184:449–454.
[9] Weidenfeller B. Internal friction studies of particulate filled polypropylene. Mater Sci Eng A. 2006;442:371–374.
[10] Birčákováá Z, Kollar P, Weidenfeller B, et al. Reversible and irreversible DC magnetization processes in the frame of magnetic, thermal and electrical properties of Fe-based composite materials. J Alloy Compd. 2015;645:283–289.
[11] Hallahan E. New thermoplastic composites for ceramic & metal replacement challenges. In: Engineering Thermoplastics 2000 Conference, Trends in Portable Electronics and Business Equipment; 2000 May; San Diego, CA.
[12] Cheng KWE, Tang CY, Cheng DKW, et al. Investigation of polymer bonded magnetic materials for power conversion. In: Proceedings of IEEE Power Electronics Specialists Conference (PESC); 2002 June 23–27; Cairns. p. 1254–1259.

[13] Asaka K. Soft magnetic materials and their applications. In: The European Conference on Powder Metallurgy – Soft Magnetic Materials Workshop; 2002 Oct; Munich. p. 45–51.
[14] Hultman L, Anderson O, Jack A. The SMC technology – from idea to reality. In: SAE International 2003 World Congress & Exhibition. 42 Volt Technology; 2003 Mar 3–6; Detroit, MI. p. 69–77.
[15] Otsuka K, Wayman CM, editors. Shape memory materials. Cambridge: Cambridge University Press; 2002.
[16] Weidenfeller B. Polymer bonded soft magnetic particles. In: Raabe D, editor. Soft Magnetic Materials 16, Vol. 2. Düsseldorf: Stahleisen; 2004. p. 797–802.
[17] Schaller R, Fantozzi G, Gremaud G, editors. Mechanical spectroscopy. Uetikon-Zuerich: Trans Tech Publications; 2001.
[18] Ward IM, Sweeney J. Mechanical properties of solid polymers. Chichester: Wiley; 2012.
[19] Ferry JD. Viscoelastic properties of polymers. 3rd ed. New York (NY): Wiley; 1980.
[20] Lambri OA. Intensidad de relajación en materiales con estructura cúbica centrada en el cuerpo [dissertation]. Rosario: Universidad Nacional de Rosario; 1993.
[21] Lambri OA. New procedure for determining internal friction parameters of tension-induced relaxation processes with distribution of relaxation times. Mater Trans JIM. 1994;35:458–465.
[22] Povolo F, Molinas BJ, Lambri OA. Influence of the moment of inertia of the pendulum on the internal friction (loss tangent) measured by free-decay. Nuovo Cimento D. 1992;14:279–286.
[23] Lambri OA, Pérez-Landazábal JI, Bonifacich FG, et al. Damping micromechanisms for bones above room temperature. J Biomim Biomater Tissue Eng. 2014;19:87–98.
[24] Lambri ML, Giordano ED, Bozzano PB, et al. Thermal degradation of type I collagen from bones. J Renew Mater. 2016;4:251–257.
[25] Niblett DH, Wilks J. Dislocation damping in metals. Adv. Phys. 1960;33:9–88.
[26] Lambri OA. A review on the problem of measuring non-linear damping and the obtainment of intrinsic damping. In: Martinez-Mardones J, Walgraef D, Woerner CH, editors. Materials instabilities. River Edge: World Scientific; 2000. p. 249–280.
[27] De Batist R. Mechanical spectroscopy. In: Lifshitz E, editor. Characterization of materials. In: Cahn RW, Haasen P, Kramer EJ, editors. Materials science and technology, Vol. 2B, Part II. Weinheim: VCH; 1991. p. 159–217.
[28] Zelada GI. Mecanismos de interacción dislocaciones-defectos puntuales en molibdeno a temperaturas entre 300 K–1300 K (0.3 TF) [Interaction mechanisms between dislocations and point defects in molybdenum at temperatures between 300K and 1300 K (0.3 Tm)]. Rosario: Universidad Nacional de Rosario; 2008.
[29] Lambri OA, Matteo CL, Mocellini RR, et al. Propiedades Viscoelásticas y Eléctricas de Sólidos y Líquidos. Una Introducción a la Electro-Reología con sus Aplicaciones Tecnológicas [Viscoelastic and electrical properties of solids and liquids. An introduction to electrorheology with their technological applications]. Rosario: UNR Editora; 2008.
[30] Lazan BJ. Damping of materials and members in structural mechanics. London: Pergamon; 1968.
[31] Lambri OA. Experimental verification of the behaviour of the different expressions for measuring amplitude dependent damping. J Phys IV. 1996;6:313–316.
[32] Molinas BJ, Povolo F. Analysis of the problem of converting measured amplitude-dependent internal friction to intrinsic values. Detailed study of the case of forced oscillations. J Phys E: Sci Instrum. 1987;20:970–977.
[33] Cullity BD. Introduction to magnetic materials. Reading: Addison-Wesley; 1972.
[34] Landau LD, Lifshitz EM. Theory of elasticity, course of theoretical physics, Vol. 7. Oxford: Pergamon Press; 1970.
[35] Abramowitz M, Stegun IA. Handbook of mathematical functions. Washington (DC): National Bureau of Standards; 1964.
[36] Friedel J. Dislocations. Oxford: Pergamon Press; 1967.
[37] Eyring H. Viscosity, plasticity, and diffusion as examples of absolute reaction rates. J Chem Phys. 1936;4:283.
[38] Glasstone S, Caidler KJ, Eyring H. The theory of the rate processes. New York (NY): McGraw Hill; 1941.

Appendix 1

In Section 'Elastic Moment Contribution', the elastic moments promoted by the matrix both for tensile and for shear states were deduced.

The expression deduced for the tensile case (18) is

$$M_{kE} = 4\pi r^3 E\left(\sqrt{1+\left(\frac{2}{\rho^2}+\frac{2}{\rho}\right)(1-\cos(\theta))}-1\right) \tag{A.1}$$

Equation (A.1) as it was already explained in Section 'Elastic Moment Contribution' is the combination of the following equations:

$$M_{kE} = 4\pi r^3 E\varepsilon \tag{A.2}$$

where

$$\varepsilon = \sqrt{1+\left(\frac{2}{\rho^2}+\frac{2}{\rho}\right)(1-\cos(\theta))}-1 \tag{A.3}$$

The equation deduced for the shear elastic moment (19) is:

$$M_{kG} = G\frac{4\pi r^3}{\rho}\theta \tag{A.4}$$

The addition of (A.1) and (A.4) gives rise to the elastic moment used in the present model (20), that is:

$$M_{G'} = M_{kE} + M_{kG} = 4\pi r^3 E\left(\sqrt{1+\left(\frac{2}{\rho^2}+\frac{2}{\rho}\right)(1-\cos(\theta))}-1\right) + G\frac{4\pi r^3}{\rho}\theta \tag{A.5}$$

Re-written (A.5) in the form:

$$M_{G'} = M_{kE} + M_{kG} = 4\pi r^3 E\varepsilon + G\frac{4\pi r^3}{\rho}\theta \tag{A.6}$$

Taking the derivative of (A.6) with respect to θ, we have:

$$\frac{dM_{G'}}{d\theta} = 4\pi r^3 E\frac{d\varepsilon(\theta)}{d\theta} + G\frac{4\pi r^3}{\rho} \tag{A.7}$$

Equation (A.7) results proportional to the Young (E) and shear (G) elastic moduli.
On the other hand, by taking the derivative of the strain given in (A.3) with respect to θ, it results:

$$\frac{d\varepsilon(\theta)}{d\theta} = \frac{1}{2}\frac{\left(\frac{2}{\rho^2}+\frac{2}{\rho}\right)\sin(\theta)}{\left(1+\left(\frac{2}{\rho^2}+\frac{2}{\rho}\right)(1-\cos(\theta))\right)^{\frac{1}{2}}} \tag{A.8}$$

Evaluating (A.8) for a typical $\rho = 0.2923$ resulting for a sample with 50% vol. magnetite (see Section 'Theoretical Background') and averaging, we can obtain $d\varepsilon(\theta)/d\theta \cong 2.9$. By replacing this value in (A.3), we obtain:

$$m_{G'} = \frac{dM_{G'}}{d\theta} = 11.6\pi r^3 E + G\frac{4\pi r^3}{\rho} \tag{A.9}$$

Then, the sum of the moments in (A.6) using the first-order term can be written as follows:

$$M_{G'} = M_{kE} + M_{kG} \cong \left(11.6\pi r^3 E + G\frac{4\pi r^3}{\rho}\right)\theta \tag{A.10}$$

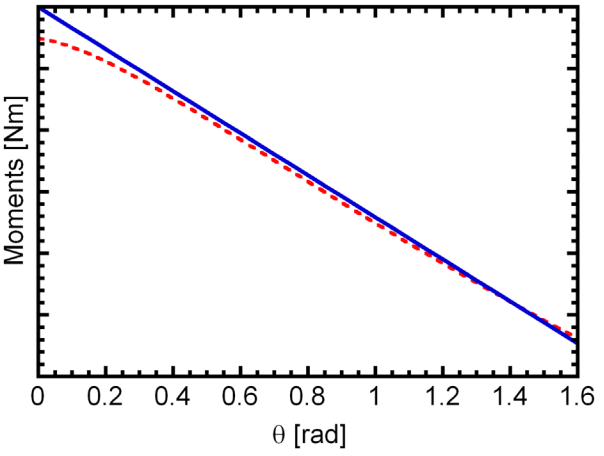

Figure 17. Behaviour of the approximated, (A.10), and the non-simplified, (A.5), Elastic Moments plotted by means of full and dashed lines, respectively.

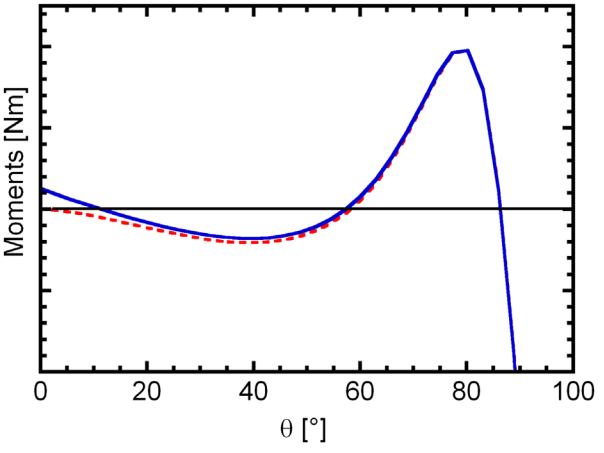

Figure 18. Behaviour of both the total intrinsic moment calculated from the linear approximation, (26), and the non-simplified expression, (25), by means of full and dashed lines, respectively.

By plotting the tensile and shear moments as a function of the torsion angle, it can be deduced that the tensile moment exhibits a linear behaviour from around 0.3 radians onwards. Therefore, in order to make easier the mathematical handling of equations a linear approximation is proposed for the sum of the two moments. Figure 17 shows the behaviour of the approximated, (A.10), and the non-simplified, (A.5), curves plotted by means of full and dashed lines, respectively.

Figure 18 shows, the behaviour of both the total intrinsic moment calculated from the linear approximation, (26), and the non-simplified expression, (25), by means of full and dashed lines, respectively. Taking into account that the present model is at mesoscopic scale, where the behaviour of the particles is averaged by a mean field approximation, a reasonably good agreement between both curves can be observed.